

When GNSS Goes Blind

Integrating Vision Measurements for Navigation in Signal-Challenged Environments

As accurate and widely available as GNSS service is, it still cannot be fully accessed everywhere, at all times, and under all conditions. In recent years, the search for seamless uninterrupted positioning, navigation, and timing has investigated a variety of other technologies that could be combined with GNSS to provide a more robust utility. This article looks into the feasibility of exploiting vision-based measurements for navigation and presents a method for using a limited number of GPS carrier phase measurements with features that are extracted from images of a monocular video camera.

ANDREY SOLOVIEV

UNIVERSITY OF FLORIDA

DONALD VENABLE

AIR FORCE RESEARCH LABORATORY, SENSORS DIRECTORATE

Photo: Integrated vision/GPS test equipment developed at the Air Force Institute of Technology (AFIT) Advanced Navigation Center (ANT)

A completely GPS-based navigation solution is generally not feasible in GNSS signal-challenged environments such as urban canyons. However, even in these difficult environments a partial set of GPS signal measurements may still be available. For instance, one or two satellites are generally still visible even in dense urban canyons.

This limited GPS ranging information is insufficient for a complete three-dimensional (3D) positioning

and timing. However, we can exploit it to improve the efficiency of alternative navigation aids such as vision-based navigation. Specifically, partial carrier phase measurements can be applied for accurate (centimeter-level) initialization of ranges to features that are extracted from video images.

Once feature ranges have been initialized, a 3D image-based navigation option is enabled and can be applied for accurate navigation in GPS-denied scenarios.

Vision-based navigation serves as a viable augmentation option to GPS. However, a fundamental limitation of vision-based approaches is the unknown range to features that are extracted from video images.

Stereo-vision methods can be used, but their performance is directly determined by the stereo baseline. This limits the application of stereo-vision for small platform cases, such as miniature unmanned aerial vehicles (UAVs) and hand-held navigation devices.

Depth information of monocular images can be initialized using platform motion to synthesize a baseline. In this approach, rather than observing a scene using two different cameras simultaneously (stereo-vision), the scene is observed sequentially from two different locations by the same camera (synthetic stereo-vision). If the synthetic baseline can be measured somehow, the image depth can be readily estimated in a manner similar to stereo-vision depth resolution.

As one option, we could measure the synthetic baseline using an inertial navigation system (INS). However, this approach leads to a correlation between inertial errors and range errors, which increases the drift of a vision-aided inertial system unless motion maneuvers are performed to decorrelate the errors.

Another method for measuring the synthetic baseline is to use GPS carrier phase measurements. GPS carrier phase provides relative ranging information that is accurate at a millimeter to sub-centimeter level. This accurate range information can be directly related to the change in platform location between images (i.e., to the synthetic baseline). Specifically, a projection of the position change vector onto the platform-to-satellite line-of-sight (LOS) unit vector is related to the change in the carrier phase between two images.


This method uses a temporal change in the carrier phase to eliminate the need for resolving integer ambiguities. Moreover, it does not require us to estimate position change from carrier phase changes first and then apply the delta position estimate for the range initialization.

As shown later in this article, carrier phase observables can be directly combined with vision observables for the accurate estimation of ranges to features that are observed by a monocular camera. In this case, the monocular image depth can be still resolved even if a limited number of GPS satellites (less than four) is available and

position change cannot be estimated.

The original motivation for vision/GPS integration was to use carrier phase for the image depth initialization. Once the image depth is resolved by estimating ranges to vision-based features, vision-only navigation remains enabled in case that GPS becomes completely unavailable.


GSG-54 GPS 8-CHANNEL SIMULATOR




GPS Constellation in a Box

Eight-Channel GPS Test Device for Manufacturing and Development

<p>Applications</p> <ul style="list-style-type: none">• Fully controllable GPS simulation• Versatile GPS functionality testing• Simulate positions, times and user movements• Standards-based GPS tests	<p>Functionality</p> <ul style="list-style-type: none">• Repeatable and reliable• Easy to use• Fast/high throughput• Affordable• Portable and compact
---	--



SPECTRACOM
Synchronizing Critical Operations®



pendulum
Test & Measurement by Spectracom

+1.585.321.5800 (North America) sales@spectracomcorp.com +46 8 598 510 00 (Europe) www.spectracomcorp.com

Join us in
SAN DIEGO



SEMINARS
MAR. 28-APR. 1, 2011

356: GPS Operations for Engineers and Technical Professionals (Mar 28/Apr 1)

Or you can select parts you need:

111: Fundamentals of GPS (Mar. 28)

122: Fundamentals and Enhancements of GPS (Mar 28-29)

217: DGPS (Mar. 30)

356B: GNSS Signals and Receiver Operations (Mar 30-Apr 1)

435: Themes in Modern GPS Receiver Architecture (Mar 30 – Apr 1)



447: Applied Kalman Filtering (Mar 28 – Apr 1)

NavtechGPS.com
(703) 256-8900
(800) 628-0885

GNSS GOES BLIND

In addition to depth resolution, accurate estimates of delta position and orientation serve as by-products of the carrier phase GPS/vision estimation algorithm. Delta position is defined as the change in the platform position vector between consecutive measurement updates. We can apply delta position estimates to reconstruct platform trajectory for applications such as guidance and control.

Research has demonstrated that delta position can be estimated at a sub-centimeter level of accuracy under open-sky GPS conditions. (See, for example, the article by F. van Graas and A. Soloviev cited in the Additional Resources section near the end of this article.) The vision/GPS method that we present here extends accurate delta position capabilities to cases of limited GPS availability.

Our algorithm also provides estimates of the camera's orientation, particularly, an estimate of the heading angle. The availability of estimated heading especially benefits integration with low-cost inertial applications where heading is not significantly observable except during acceleration and/or turning maneuvers.

This article focuses on use of the GPS/vision integration approach for the case of point features. However, the approach can be generalized for other feature representations (such as, for example, line features or planar surfaces).

GPS/vision estimation can operate under a very limited GPS availability. Specifically, it only requires one satellite if the receiver clock has previously been initialized and the camera's orientation is known. Two satellites are needed for the case of a calibrated clock but unknown orientation, and three satellites are required if both clock and orientation are unknown.

In this article, we will first offer a conceptual explanation of the GPS/vision integration method followed by a complete formulation of the estimation routine. Finally, we will provide simulation results and initial field test results to validate the proposed algorithm and demonstrate its performance characteristics.

Concept

The carrier phase/vision range initialization approach is based on observing vision-based features from two different locations of the platform. The problem of using video features alone is that vision measurement observables that relate changes in feature parameters with changes in navigation parameters and unknown feature ranges are homogeneous. These homogeneous observables can only be resolved within the ambiguity of a scale-factor.

Incorporation of GPS carrier phase measurements adds a non-homogeneous observation component that allows us to remove the scale-factor ambiguity. To illustrate, consider a simplified case of translational motion only. In this case, change in the platform position vector and unknown feature ranges are related as follows:

$$\mathbf{H}_k \cdot \begin{bmatrix} \Delta \mathbf{R} \\ Z_k^{(1)} \end{bmatrix} = \mathbf{0}_{2 \times 1}, k = 1, \dots, K \quad (1)$$

where: $\Delta \mathbf{R}$ is the position change vector between images (1) and (2); $Z_k^{(1)}$ is the unknown range to the feature k for image (1); matrix \mathbf{H}_k is defined by the homogeneous coordinates of point features that are extracted from images (1) and (2); $\mathbf{0}_{2 \times 1}$ is the 2 by 1 zero vector; and K is the total number of features.

Equation (1) is a homogeneous system of linear equations. For (i.e., when the number of unknowns, which is $K+3$ is less than the number of equations, which is $2K$), this system can be resolved into position and range estimates, but only within the ambiguity of a scale-factor — that is, if a specific solution satisfies the system its scaled version will satisfy the system as well.

GPS carrier phase measurements provide non-homogeneous measurement observables that allow removal of the scale-factor ambiguity. Using a procedure described in the previously cited article by F. van Graas et alia, changes in carrier phase measurements between images (1) and (2) are related to the platform position change as follows:

$$\Delta \phi_p = -(\mathbf{e}_p, \Delta \mathbf{R}) + c \Delta t_{rcvr}, p = 1, \dots, P \quad (2)$$

where $\Delta \phi_p$ is the carrier phase change; \mathbf{e}_p is the satellite/platform line-of-sight unit vector; (\cdot) is the vector dot product; Δt_{rcvr} is the receiver clock drift that is accumulated between images (1) and (2); c is the speed of light; and, P is the number of visible satellites.

Note that carrier phase changes in Equation (2) are assumed to be compensated for the satellite motion and changes in relative platform/satellite geometry as described in the following section.

Equation (1) combined with Equation (2) defines a system of linear equations that can be unambiguously resolved into position changes and range estimates. We can use the solution of this combined system to initialize ranges of video-based features. In addition, the delta position vector $\Delta \mathbf{R}$ is estimated.

Note that the integrated GPS/vision range initialization does not require the resolution of integer carrier ambiguities because differencing of carrier phase measurements removes the ambiguity component. We should also point out that the combined use of equations (1) and (2) assumes that the platform's frame at image (1) is aligned with the global reference frame. This assumption is eliminated in the general case, which uses an estimate of the platform's initial attitude. We will consider the general case further in the next section.

To summarize the foregoing description of the simplified case, **Figure 1** shows a generalized diagram of the GPS/vision estimation routine.

Temporal changes in the GPS carrier phase are combined with vision measurements (image-based coordinates of point features) to initialize unknown ranges to vision-based features. In addition to range initialization, the integrated solution estimates delta position and (in a general case of unknown camera orientation) the orientation of the camera's body-frame relative to the global navigation frame of reference.

NavtechGPS

SINCE 1984

YOUR ONE SOURCE FOR GPS HARDWARE.

The choices you want.
The experience you need.



NavtechGPS.com
(703) 256-8900
(800) 628-0885

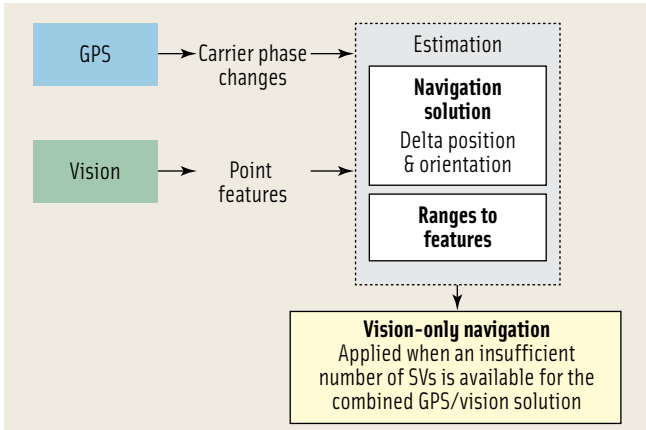


FIGURE 1 Generalized GPS/vision estimation routine

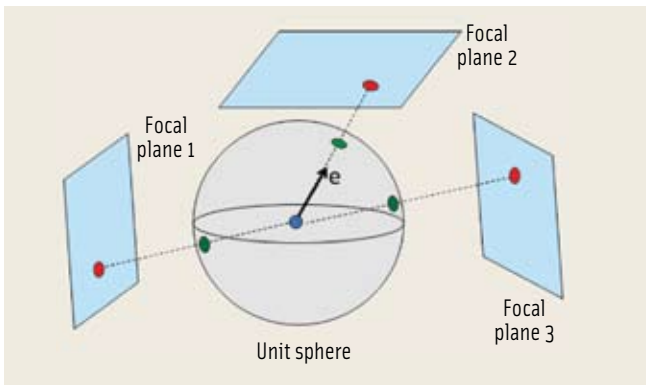


FIGURE 2 Unit sphere representation of features for multi-aperture camera case

GPS/Vision Estimation Approach

This section formulates the carrier phase GPS/vision solution for the general six-degrees-of-freedom (6 DOF) motion case. First, vision observables of the estimation algorithm are formulated. Next, we provide the GPS observation equations and then describe the estimation algorithm.

Vision observables. Vision observables are formulated for the general case of multi-aperture vision. In this case, video images are recorded by multiple camera apertures. As compared to cases of single aperture, the multi-aperture formulation has a number of advantages including improved situational awareness, increased number of high-quality features, and a better feature geometry. These advantages are discussed further in the article by A. Soloviev et alia cited in Additional Resources.

Features that are observed in focal planes of individual cameras are first projected onto the surface of a unit sphere that serves as a unified frame of reference. Figure 2 illustrates this projection.

Essentially, the unit sphere projection represents a feature as a unit vector with its associated azimuth and elevation angles. We choose the unit sphere representation because it does not suffer from singularity cases as opposed to a Cartesian representation where projection singularities can exist.

Motion constraints relate coordinates of features (spherical angles and their corresponding unit vectors) that are observed in images (1) and (2) to changes in platform position and orientation between these two images. For a general 3D case that includes translational and rotational motion components, two motion constraint equations are derived:

$$\begin{aligned} & \left(\mathbf{e}_k^{(2)} \right)^T \cdot \Delta \mathbf{C}_N^b \cdot \mathbf{B} \cdot \Delta \mathbf{R}^b - \left(\mathbf{e}_k^{(1)} \right)^T \cdot \mathbf{B}^T \cdot \Delta \mathbf{C}_b^N \cdot \mathbf{e}_k^{(2)} \cdot \rho_k^{(1)} = 0 \\ & \left(\mathbf{e}_k^{(2)} \right)^T \cdot \Delta \mathbf{C}_N^b \cdot \mathbf{D} \cdot \Delta \mathbf{R}^b - \left(\mathbf{e}_k^{(2)} \right)^T \cdot \Delta \mathbf{C}_N^b \cdot \mathbf{e}_{\perp k}^{(1)} \cdot \rho_k^{(1)} = 0 \end{aligned} \quad (3)$$

$k = 1, \dots, K$

where:

$\rho_k^{(1)}$ is the distance to the feature k for image (1) (This distance is the unknown feature range that is sought to be initialized.); $\mathbf{e}_k^{(m)}$ is the unit vector of feature k for image m ($m=1,2$), and $\mathbf{e}_{\perp k}^{(m)}$ is the unit vector perpendicular to $\mathbf{e}_k^{(m)}$;

$\Delta \mathbf{R}^b$ is the change in position vector between images (1) and (2) with vector components resolved in the camera's body-frame; $\Delta \mathbf{C}_b^N$ is the change in the body-to-navigation frame direction cosine matrix (DCM) between images (1) and (2); this change is defined as the direction cosine matrix for the coordinate transformation that aligns body frame at image (1) with body-frame at image (2), i.e. $\Delta \mathbf{C}_b^N = \mathbf{C}_{b_1}^{b_2}$;

K is the number of features, and matrices \mathbf{B} and \mathbf{D} are defined as follows:

$$\mathbf{B} = \begin{bmatrix} 0 & -1 & 0 \\ 1 & 0 & 0 \\ 0 & 0 & 0 \end{bmatrix} \quad (4)$$

$$\mathbf{D}_k = \begin{bmatrix} 0 & 0 & -\cos(\varphi_k^{(1)}) \\ 0 & 0 & -\sin(\varphi_k^{(1)}) \\ \cos(\varphi_k^{(1)}) & \sin(\varphi_k^{(1)}) & 0 \end{bmatrix}$$

where φ is the spherical azimuth angle.

We assume that the estimate of the orientation change matrix $\Delta \mathbf{C}_b^N$ is provided by the INS. In the 6 DOF case, the system expressed in Equation (3) is a linear system of homogeneous equations with regard to the position change vector $\Delta \mathbf{R}^b$ and unknown feature ranges.

Similar to the simplified case considered in the previous section, such a system does not have a unique solution: if a certain solution satisfies the system, then its scaled version satisfies the system as well. To resolve the scale-factor ambiguity, non-homogeneous measurement observations are added by using the GPS carrier phase.

GPS Observables. The GPS carrier phase measurement is expressed as:

$$\tilde{\varphi}_p = \rho_p + \lambda N_p + c\delta t_{rcvr} + \varepsilon_p + \eta_p \quad (5)$$

$p = 1, \dots, P$

where:

$\tilde{\varphi}_p$ is the measured carrier phase for satellite p ;

ρ_p is the true range between the receiver and the satellite;

λ is the carrier wavelength;
 N_p is the integer ambiguity;
 c is the speed of light;
 δt_{rcvr} is the receiver clock bias;
 ϵ_p is the deterministic error term that incorporates ionospheric and tropospheric delay errors and satellite orbital error;
 η_p is the combined noise and multipath term; and,
 P is the number of visible satellites.

Equation (5) assumes that the satellite clock bias is compensated using ephemeris data.

As mentioned previously, temporal carrier phase changes are applied for GPS/vision integration. From (5), the temporal phase change is expressed as follows:

$$\Delta\tilde{\varphi}_p = \tilde{\varphi}_p(t_2) - \tilde{\varphi}_p(t_1) = \Delta\rho_p + c\Delta\delta t_{rcvr} + \Delta\eta_p \quad (6)$$

$p = 1, \dots, P$

where time instances t_1 and t_2 correspond to images (1) and (2).

Carrier phase differencing over time removes the constant integer ambiguity term. In addition, change in the deterministic error term ϵ generally stays below a centimeter/second level. This term is therefore neglected. The change in the true range $\Delta\rho$ is directly related to the change in the platform position. The range change equation is obtained by considering the satellite-receiver geometry that is shown in **Figure 3**.

From Figure 3 the following relationship is derived:

$$\begin{aligned} \Delta\rho &= \rho(t_2) - \rho(t_1) \\ &= (\mathbf{R}_{SV}(t_2) - \mathbf{R}(t_2), \mathbf{e}(t_2)) - (\mathbf{R}_{SV}(t_1) - \mathbf{R}(t_1), \mathbf{e}(t_1)) \quad (7) \\ &= -(\mathbf{e}(t_2), \Delta\mathbf{R}) \\ &\quad + (\mathbf{R}_{SV}(t_2), \mathbf{e}(t_2)) - (\mathbf{R}_{SV}(t_1), \mathbf{e}(t_1)) \\ &\quad - (\Delta\mathbf{e}(t_2), \mathbf{R}(t_1)) \end{aligned}$$

where:

\mathbf{R}_{SV} is the satellite position vector;
 \mathbf{R} is the platform position vector;
 $\Delta\mathbf{R}$ is the platform position change vector; note that components of this vector are resolved in the global navigation frame; and,
 \mathbf{e} is the satellite-to-platform LOS unit vector.

The term $(\mathbf{R}_{SV}(t_2), \mathbf{e}(t_2)) - (\mathbf{R}_{SV}(t_1), \mathbf{e}(t_1))$ is due to the satellite motion along the LOS. This term is referred to as the SV (space vehicle) Doppler term. The term $(\Delta\mathbf{e}(t_2), \mathbf{R}(t_1))$ stems from changes in the LOS orientation and is referred to as geometry change.

SV Doppler and geometry change are independent of the position change and, therefore, are compensated based on the approximate knowledge of the platform position and satellite ephemeris data. Note that this compensation uses an estimated platform position. This estimate has to be accurate only within 100 meters.

Carrier phase measurements that are adjusted for SV Doppler and geometry changes serve as GPS observables of the combined GPS/vision estimation:

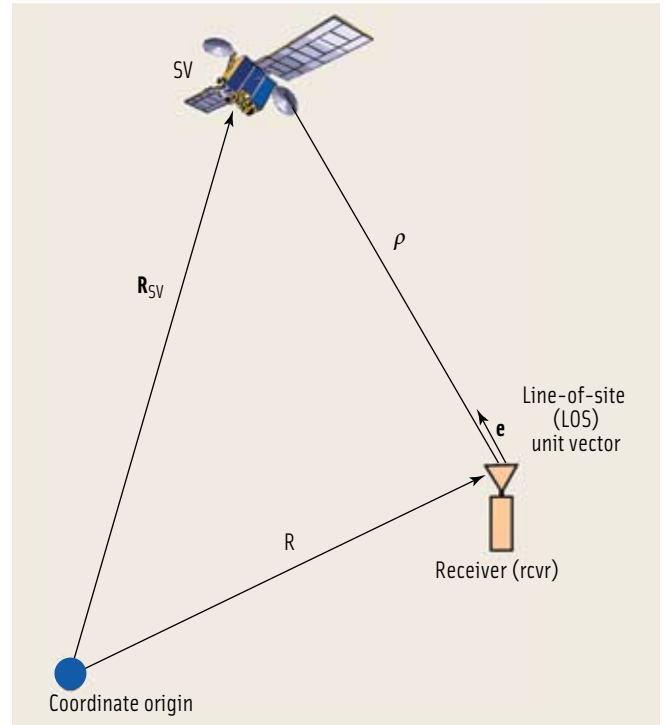


FIGURE 3 Satellite-receiver geometry

$$\Delta\tilde{\varphi}_p^{adj} = -(\mathbf{e}(t_2), \Delta\mathbf{R}) + c\Delta\delta t_{rcvr} + \Delta\eta_p \quad (8)$$

$p = 1, \dots, P$

Estimation procedure.

The estimation procedure combines vision and GPS measurement observables that are formulated by equations (3) and (8), accordingly. Note that the position change vector in Equation (3) is resolved in the camera body frame, while the same vector in Equation (8) is resolved in the axes of navigation frame. To convert both vision and GPS observations into the same frame of reference, GPS observables are transformed into the body-frame and the final combined observation equation is expressed as follows:

$$\begin{aligned} (\mathbf{e}_k^{(2)})^T \cdot \Delta\mathbf{C}_N^b \cdot \mathbf{B} \cdot \Delta\mathbf{R}^b - (\mathbf{e}_k^{(1)})^T \cdot \mathbf{B}^T \cdot \Delta\mathbf{C}_N^b \cdot \mathbf{e}_k^{(2)} \cdot \rho_k^{(1)} &= 0 \\ (\mathbf{e}_k^{(2)})^T \cdot \Delta\mathbf{C}_N^b \cdot \mathbf{D} \cdot \Delta\mathbf{R}^b - (\mathbf{e}_k^{(2)})^T \cdot \Delta\mathbf{C}_N^b \cdot \mathbf{e}_{\perp k}^{(1)} \cdot \rho_k^{(1)} &= 0 \quad (9) \end{aligned}$$

$k = 1, \dots, K$

$$\Delta\tilde{\varphi}_p^{adj} = -(\mathbf{C}_N^b \mathbf{e}(t_2), \mathbf{C}_N^b \Delta\mathbf{R}^b) + c\Delta\delta t_{rcvr} + \Delta\eta_p$$

$p = 1, \dots, P$

where \mathbf{C}_N^b is the DCM for the transformation from navigation frame to body frame.

Equation (9) defines a non-homogeneous system of equations that can be uniquely resolved into feature ranges, position change vector, and orientation, assuming that a sufficient number of measurement observations exist. The DCM matrix \mathbf{C}_N^b is uniquely defined by pitch, roll, and heading angles of the platform.

Pitch and roll angles are observable in the GPS/INS integrated mechanization. These angles can be accurately measured (at a milliradian level) by the INS that is calibrated with GPS

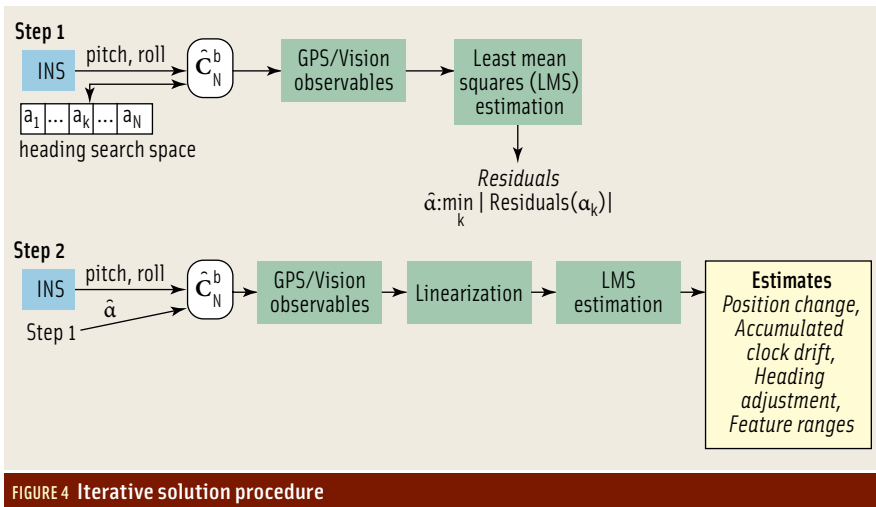


FIGURE 4 Iterative solution procedure

carrier phase even for cases of low-cost inertial and limited GPS availability. Therefore, it is assumed that pitch and roll estimates are provided by the INS.

The use of this assumption reduces the minimum number of satellites required for the GPS/vision estimation from five to three. Heading angle is poorly observable and is, therefore, included as an unknown in the GPS/vision estimation routine.

The equation system (9) is non-linear with regard to angular orientation. Therefore, an iterative solution procedure is applied as illustrated in Figure 4.

The first step finds an initial (approximate) value of heading. This step searches through all possible values of heading angle. A 0-to-360-degree search with a search grid of 5 degrees is currently being implemented. For each heading angle from the search space, an estimate of the DCM is computed and applied in Equation (9). As a result, Equation (9) becomes a linear system of equations with regard to position change vector, accumulated receiver clock drift ($\Delta\delta t_{\text{recv}}$), and feature ranges.

This system is resolved by using the least mean square (LMS) solution procedure, followed by calculation of solution residuals. We determined empirically that the LMS residual norm has a global minimum that corresponds to the true heading value. Therefore, we chose the heading angle that minimizes LMS solution residuals as the initial heading estimate.

The second iteration linearizes GPS

observables around the initial heading estimate and then implements the linear LMS solution to compute position change, accumulated clock drift, adjustment to the initially estimated heading, and feature ranges. The LMS herein is implemented as a weighted procedure that weights measurement observables according to their quality measured by

the — covariances of vision measurement errors and carrier phase measurement noise.

Note that position change estimates are resolved in the camera body frame. Therefore, they are transformed into the global navigation frame using the C_N^b matrix that is constructed based on INS pitch and roll angles and the heading estimate that is computed as described earlier.

For a general case of unknown receiver clock and heading angle, at least three satellites are required to achieve a full-rank of the equation system (9): one satellite for partial observability of delta position (i.e., to enable at least one non-homogeneous relationship for the resolution of delta position components), one satellite to resolve the accumulated clock drift, and one satellite for the heading observability.

In this case, the number of unknowns is $K+5$ (K feature ranges, 3 delta position components, clock, and heading angle)

TURN TO PCTEL FOR APPLICATION-FOCUSED GPS/SATCOM ANTENNA SOLUTIONS

PCTEL designs and manufactures high performance antennas to provide precise operation, maximum durability, and ease of installation for applications in:

- Network Timing
- Vehicle/Asset Tracking
- Public Safety
- Military
- Satellite Communications
- Aviation
- Precision Measurement
 - Agriculture
 - Construction

For your custom, application-specific, GPS/SATCOM antenna designs contact the PCTEL sales team.

A LEADING PROVIDER OF HIGH PERFORMANCE GPS/SATCOM ANTENNAS

PCTEL™
simplifying mobility

phone 630.372.6800
toll-free 800.323.9122
website <http://antenna.com>
email antenna.sales@pctel.com

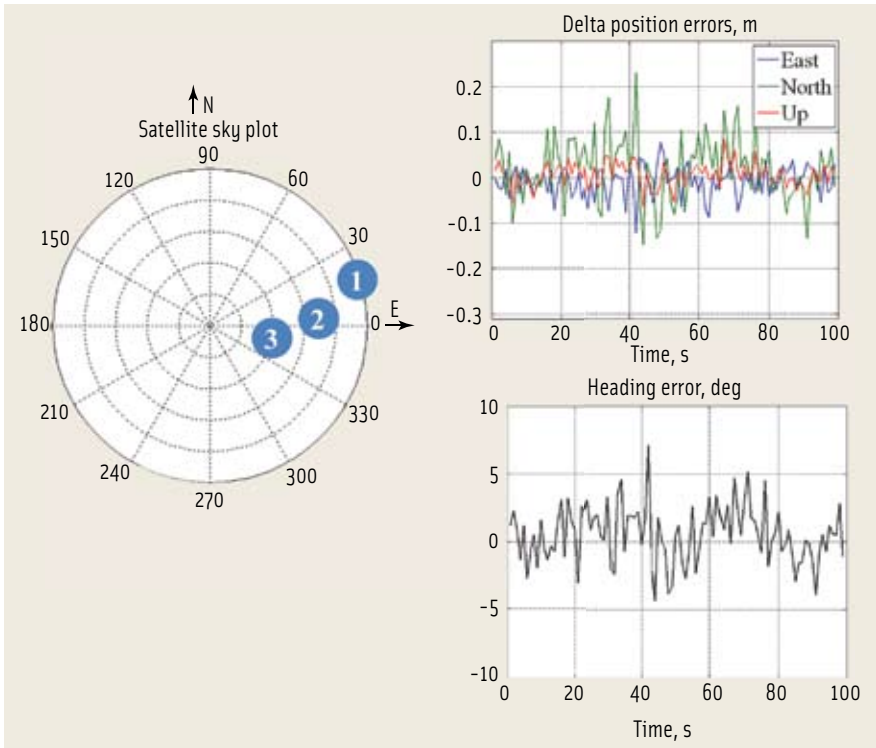


FIGURE 5 Simulation results for Scenario 1: 3 SVs with poor geometry

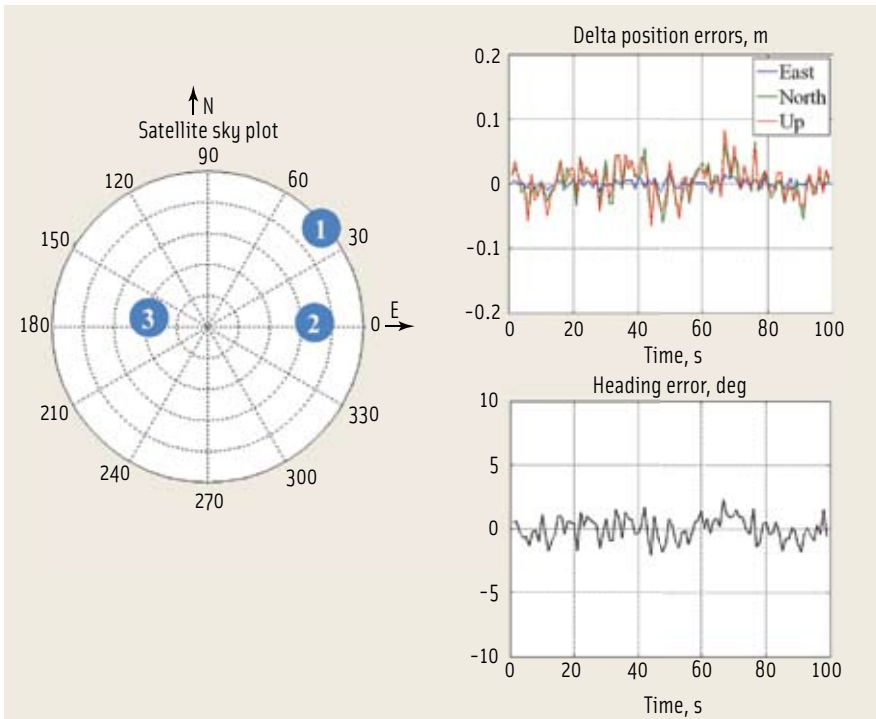


FIGURE 6 Simulation results for Scenario 2: 3 SVs with good geometry

of satellites can be reduced to two if the receiver clock is pre-calibrated and to one if both receiver clock and heading angle are known *a priori*.

Test Results

This section presents simulation results and initial experimental results that validate the GPS/vision integrated solution and evaluate its performance characteristics.

Simulation results. The following simulation scenario was implemented:

- Motion scenario: straight motion with a two meter/second velocity
- GPS measurements: carrier phase with five-millimeter (one sigma) noise
- Vision: multi-aperture vision system — four cameras with mutually orthogonal axes, 40×30-degree field of view, and 640×480 resolution;
- Vision features: 10 features uniformly distributed over the multi-aperture field of view;
- Feature measurement noise: one pixel (sigma)
- Inertial: lower-cost inertial unit — 0.1 degree/second (360 degree/hour) gyro drift
- Algorithm update rate: one update per second

Note that the simulation results reported here were generated for the case of a multi-aperture camera system. However, we observed that the increased number of apertures does not have a noticeable influence on the overall system performance. Therefore, similar results can be expected for single-aperture implementation.

Figures 5 through 8 show simulation results for several examples of simulation scenarios. **Figure 5** shows simulation results for Simulation Scenario 1. In this case, three visible satellites are generated with poor satellite geometry as shown in Figure 5. This satellite geometry is representative for a narrow urban canyon.

Scenario 1 achieved a sub-decimeter delta positioning accuracy. The heading estimates are accurate at a degree-level. Standard deviations of estimation errors were computed as follows:

and the number of equations is $2K+3$. Therefore, only two vision features are required to uniquely resolve the system. However, we do not recommend the use of this minimum required number

of features as it generally leads to poor state observability. The availability of at least 5 to 10 features is desirable to support adequate estimation accuracy. It is noted that the minimum number

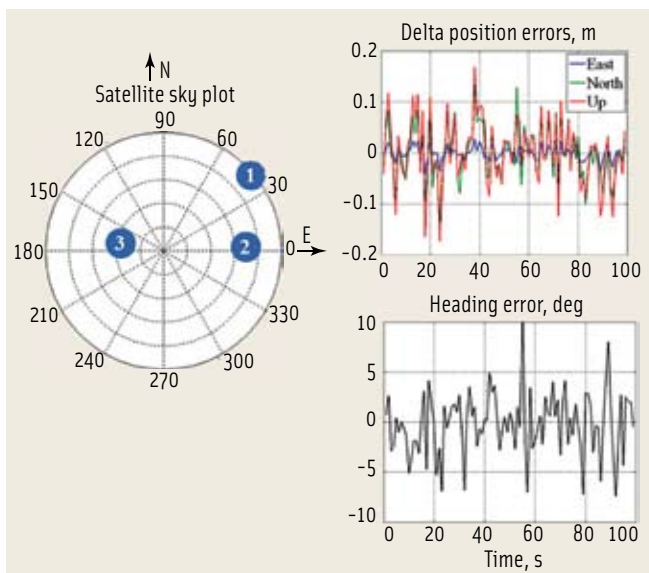


FIGURE 7 Simulation results for Scenario 3: 3 SVs with good geometry; reduced quality of inertial sensors (consumer-grade gyro measurements with a 0.5 deg/s drift are simulated)

- East delta position error (sigma): 3.43 centimeters
- North delta position error (sigma): 6.99 centimeters
- Vertical delta position error (sigma): 2.64 centimeters
- Heading error (sigma): 2.12 degrees.

Figure 6 shows simulation results for Scenario 2.

In this case, we implemented an improved satellite geometry. As a result, a factor 2 to 5 error reduction was achieved for horizontal delta position and heading error components. Particularly, the error standard deviations were evaluated as follows:

- East delta position error (sigma): 0.63 centimeters
- North delta position error (sigma): 2.53 centimeters
- Vertical delta position error (sigma): 2.65 centimeters
- Heading error (sigma): 0.94 degrees.

Figure 7 shows simulation results for Scenario 3. We designed this scenario to illustrate the influence of inertial sensor errors on the estimation performance. We applied a good satellite geometry that corresponds to the previous simulation scenario (Scenario 2) and simulated measurements of consumer-grade gyros with a 0.5 degree/second drift rate.

As formulated in the previous section, we used gyro measurements to compensate for the orientation changes between consecutive images (see Equation (3) above). We did this in order to exclude angular changes from estimated states and to keep the vision measurement observables linear.

However, due to the use of gyro measurements, gyro drifts transform into vision observation errors and then into estimation errors. As a result, a degradation of the gyro drift performance from 0.1 degree/second to 0.5 degree/second leads to a



PTTI 2010
www.pttimeeting.org

15-18 November 2010
 Hyatt Regency Hotel
 Reston Town Center, Virginia

Have you reserved your booth space for PTTI 2010?
 Booth space may be limited.

Credit cards are accepted.

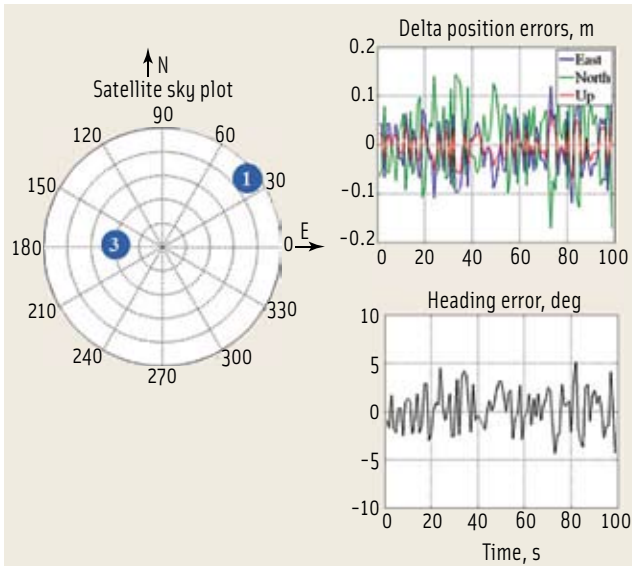


FIGURE 8 Simulation results for Scenario 4: 2 SVs, pre-calibrated receiver clock

factor 2 to 3 decrease in the estimation accuracy. Particularly, the estimation errors for Scenario 3 were evaluated as follows:

- East delta position error (sigma): 1.39 centimeters
- North delta position error (sigma): 5.04 centimeters
- Vertical delta position error (sigma): 6.27 centimeters
- Heading error (sigma): 3.08 degrees.

Finally, **Figure 8** shows simulation results for Scenario 4. In this case, the receiver clock is pre-calibrated. As a result, only two satellites can be used. The gyro drift is improved to its original number of 0.1 degree/second.

As shown in **Figure 8**, the system states can be still estimated when only two satellites are available if the receiver clock is pre-calibrated. The accuracy performance is reduced as compared to the case of three-SV availability and an uncalibrated clock. Specific accuracy numbers were evaluated as:

- East delta position error (sigma): 5.28 centimeters
- North delta position error (sigma): 7.53 centimeters
- Vertical delta position error (sigma): 2.91 centimeters
- Heading error (sigma): 2.13 degrees.

Experimental results. **Figure 9** depicts the experimental data collection setup.

This setup was developed at the Advanced Navigation Technology (ANT) Center at the Air Force Institute of Technology (AFIT) and used the following equipment for the GPS/vision experiment:

- a 24-channel, dual-frequency GPS receiver
 - Vision:
 - one-camera system
 - 45-degree horizontal field of view
 - 1280x1024 resolution
 - Feature measurement noise: 1 pixel (sigma)
 - SURF feature extraction
 - Inertial:
 - Lower-cost inertial unit: 0.5 deg/s (1800 deg/hr) gyro drift
- The test trajectory implemented includes straight motion

segments with one meter/second velocity and low dynamic turns. **Figure 10** illustrates a method that was applied for the evaluation of the integrated GPS/vision performance with experimental data.

Experimental data were collected under open sky and partially obstructed GPS conditions. The original satellite constellation that includes five or more SVs was artificially reduced to three satellites in order to test the GPS/vision algorithm. A GPS-only delta position that was computed from carrier phase changes of the original satellite constellation served as the reference trajectory. As shown in the article by F. van Graas and A. Soloviev, this reference trajectory is accurate at a mm-level.

Figure 11 shows experimental results.

Delta position error sigmas were computed as follows:

- East delta position error (sigma): 1.55 centimeters;
- North delta position error (sigma): 5.81 centimeters;
- Vertical delta position error (sigma): 7.87 centimeters;

These performance figures agree with the evaluated system performance for the simulation Scenario 3, which simulated a consumer-grade inertial with a 0.5 degree/second gyro drift (i.e., the same gyro performance as in the case of the experiment) and a three-SV satellite constellation.

Overall, simulation results and initial test results presented in this section demonstrate the validity of the integrated GPS/vision estimation approach. The results show delta position estimation that is accurate at a centimeter to sub-decimeter level and heading estimation accuracy in a range from one to three degrees.

Conclusions

This paper proposes the integration of partial GPS measurements with vision-based features for navigation in GPS-challenged environments where a stand-alone GPS navigation solution is not feasible. The integration routine developed estimates changes in platform delta position, the platform's heading angle and initializes ranges to features of monocular video camera. Simulation results and initial test results demonstrate the efficacy of the vision/GPS data fusion algorithm.

Future work will focus on detailed evaluations with experimental data including transitions between partial GPS and GPS-denied environments. Future work will also consider fusion of vision and GPS for the estimation of absolute position states (rather than delta position) under a limited satellite availability.

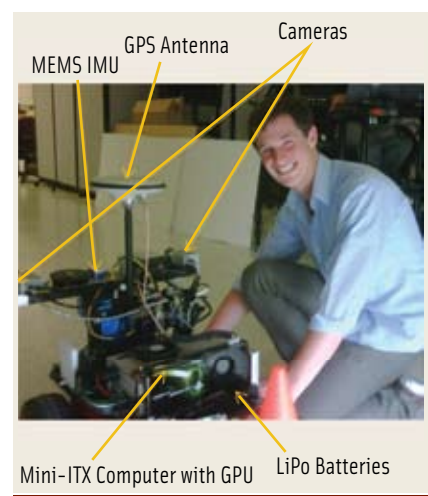


FIGURE 9 Experimental setup

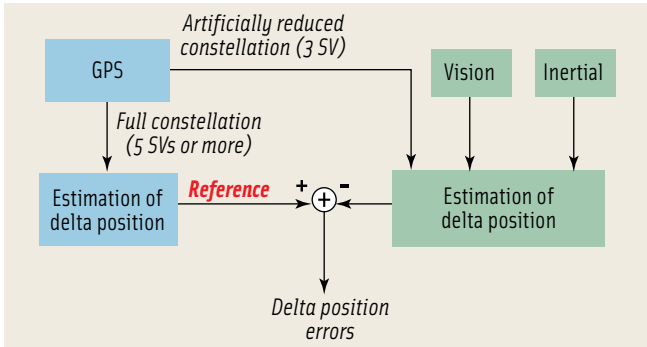


FIGURE 10 Method applied for the GPS/vision performance evaluation with experimental data

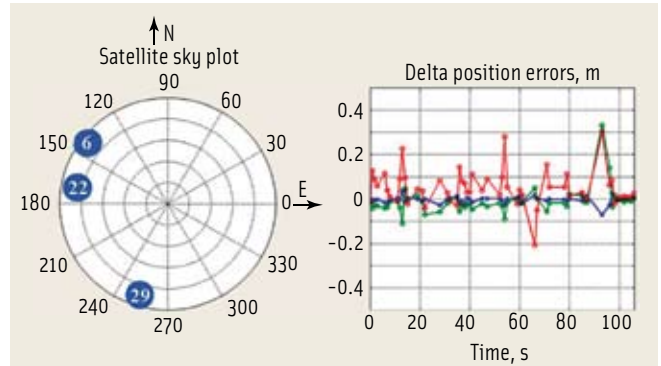


FIGURE 11 Experimental results

Acknowledgement

This article is based on a paper presented at the 2010 Position Location and Navigation Symposium (PLANS 2010), copyright IEEE. The authors would like to thank the ANT Center at AFIT for providing the data collection setup.

Manufacturers

The experimental data collection system used in the tests incorporated an OEM4 GNSS receiver from **NovAtel, Inc.**, Calgary, Alberta, Canada, and PL-A741 video cameras from **PixelLINK**, Ottawa, Ontario, Canada, and a MIDG II IMU from **Microbotics, Inc.**, Hampton, Virginia, USA.

References

- [1] Kaplan, E., and C. Hegarty (Editors), *Understanding GPS: Principles and Applications*, 2nd ed., Artech House, Norwood, Massachusetts, USA, 2006
- [2] Soloviev, A., "Tight Coupling of GPS, Laser Scanner, and Inertial Measurements for Navigation"
- [3] Soloviev, A., and J. Touma, T. J. Klausutis, A. Rutkowski, and K. Fontaine, "Integrated Multi-Aperture Sensor and Navigation Fusion," in *Proceedings of the Institute of Navigation GNSS-2009*, September 2009 in Urban Environments," *Proceedings of IEEE/ION Position Location and Navigation Symposium*, May 5-8, 2008, Monterey, California
- [4] van Graas, F., and A. Soloviev, "Precise Velocity Estimation Using a Stand-Alone GPS Receiver," *NAVIGATION*, Journal of the Institute of Navigation, Vol. 51 No. 4, 2004
- [5] Veth, M. J., "Fusion of Imaging and Inertial Sensors for Navigation," Ph.D. dissertation, Air Force Institute of Technology, September, 2006

Authors



Andrey Soloviev is a research assistant professor at the University of Florida. Previously he served as a senior research engineer at the Ohio University Avionics Engineering Center. He holds B.S. and M.S. degrees in applied mathematics and physics from Moscow University of Physics and Technology and a Ph.D. in electrical engineering from Ohio University. His research interests focus on all aspects of multi-sensor integration for navigation including integrated processing of GPS, inertial, laser radar, and imagery signals. Soloviev received the RTCA William E. Jackson Award in 2002 and the Institute of Navigation Early Achievement Award in 2006.



Donald Venable is an associate electronics engineer at the Air Force Research Laboratory, Reference Systems Branch, at Wright Patterson AFB, Ohio. He received his B.S. and M.S. degrees in electrical engineering from Ohio University while a research associate for the Ohio University Avionics Engineering Center. During his studies, he also was a cooperative education student working for the Honeywell Aerospace Guidance and Navigation division. His research interests are focused on the areas of image and ranging sensor-aided navigation, cooperative navigation, and other techniques for navigating in GNSS-challenged environments.